



Article

Electrostatic Self-Assembly of Diamond Nanoparticles onto Al- and N-Polar Sputtered Aluminum Nitride Surfaces

Taro Yoshikawa ^{1,*}, Markus Reusch ^{1,2}, Verena Zuerbig ¹, Volker Cimalla ¹, Kee-Han Lee ³, Magdalena Kurzyp ³, Jean-Charles Arnault ³, Christoph E. Nebel ¹, Oliver Ambacher ^{1,2} and Vadim Lebedev ¹

¹ Fraunhofer Institute for Applied Solid State Physics, Tullastraße 72, 79108 Freiburg, Germany; markus.reusch@iaf-extern.fraunhofer.de (M.R.); verena.zuerbig@iaf.fraunhofer.de (V.Z.); volker.cimalla@iaf.fraunhofer.de (V.C.); christoph.nebel@iaf.fraunhofer.de (C.E.N.); oliver.ambacher@iaf.fraunhofer.de (O.A.); vadim.lebedev@iaf.fraunhofer.de (V.L.)

² Department of Microsystems Engineering—IMTEK, University of Freiburg, Georges-Köhler-Allee 103, 79110 Freiburg, Germany

³ Atomic Energy and Alternative Energies Commission (CEA), Laboratory of Applied Research on Software-Intensive Technologies (LIST), Diamond Sensors Laboratory, F-91191 Gif-sur-Yvette, France; keehan.lee@cea.fr (K.-H.L.); magdalena.kurzyp@cea.fr (M.K.); jean-charles.arnault@cea.fr (J.-C.A.)

* Correspondence: taro.yoshikawa@iaf.fraunhofer.de; Tel.: +49-761-5159-642

Academic Editor: Qiaoqin Yang

Received: 11 October 2016; Accepted: 10 November 2016; Published: 17 November 2016

Abstract: Electrostatic self-assembly of diamond nanoparticles (DNPs) onto substrate surfaces (so-called nanodiamond seeding) is a notable technique, enabling chemical vapor deposition (CVD) of nanocrystalline diamond thin films on non-diamond substrates. In this study, we examine this technique onto differently polarized (either Al- or N-polar) *c*-axis oriented sputtered aluminum nitride (AlN) film surfaces. This investigation shows that Al-polar films, as compared to N-polar ones, obtain DNPs with higher density and more homogeneously on their surfaces. The origin of these differences in density and homogeneity is discussed based on the hydrolysis behavior of AlN surfaces in aqueous suspensions.

Keywords: electrostatic self-assembly; nanodiamond seeding; diamond nanoparticles; aluminum nitride; polarity; surface oxidation; hydrolysis; zeta potential

1. Introduction

Chemical vapor deposition (CVD) of nanocrystalline diamond (NCD) on aluminum nitride (AlN) is an epochal approach to combine NCD and AlN [1]. This approach responds well to the demand for NCD/AlN unimorph structures used in surface acoustic wave resonators [2], mechanical micro-resonators [3], and tunable micro-optical lenses [4] since it has a potential to obtain homogeneous NCD thin films on *c*-axis oriented sputtered AlN films. The vital step of this approach is the nucleation enhancement of diamond on AlN surfaces prior to the CVD process because the nucleation density on pure (untreated) AlN surfaces is extremely low (10^6 – 10^7 cm⁻²) [5]. To date, some different surface pretreatments of AlN have been examined to enhance diamond nucleation, e.g., hot-filament irradiation in a hydrogen atmosphere [6], negative bias treatment [7], and electrostatic self-assembly of diamond nanoparticles (DNPs) (more commonly known as nanodiamond seeding) [1]. Among them all, electrostatic self-assembly of DNPs appears to be the most promising method for all of the applications introduced above due to its potential to supply an extremely high density ($>10^{11}$ cm⁻²) of DNPs homogeneously on AlN surfaces as diamond nucleation sites, enabling the deposition of ultra-thin

(~40 nm) and highly homogeneous (root mean square (rms) surface roughness of 12 nm) NCD films on them [1]. Owing to such an excellent potential, some systematic studies concerning electrostatic self-assembly of DNPs onto AlN surfaces have been done. For example, Hees et al. investigated the influence of pH in aqueous colloids of DNPs on the density of DNPs assembled onto AlN surfaces. This investigation revealed that the relationship of zeta potentials between DNPs and AlN surfaces dominates the electrostatic attractive interaction between them during the electrostatic self-assembly process [1]. Also, Pobedinskas et al. studied the effect of plasma treatment of AlN surfaces on the density of DNPs assembled onto AlN surfaces. This study clarified that the electrical charges and chemical groups of AlN surfaces strongly influence the adhesion between DNPs and AlN surfaces [8]. One important conclusion that can be drawn from these studies is that the surface properties of both DNPs and AlN are the crucial factors for electrostatic self-assembly of DNPs onto AlN surfaces. Now, *c*-axis oriented sputtered AlN films can be either Al- or N-polar, resulting in different surface terminations as the models of crystal structures for both Al- and N-polar cases are shown in Figure 1. Since such differently polarized AlN films naturally have different surface properties, e.g., electrical charge [9] and chemical reactivity [10–12], the polarity of AlN films would also be an influential factor for electrostatic self-assembly of DNPs onto AlN surfaces.

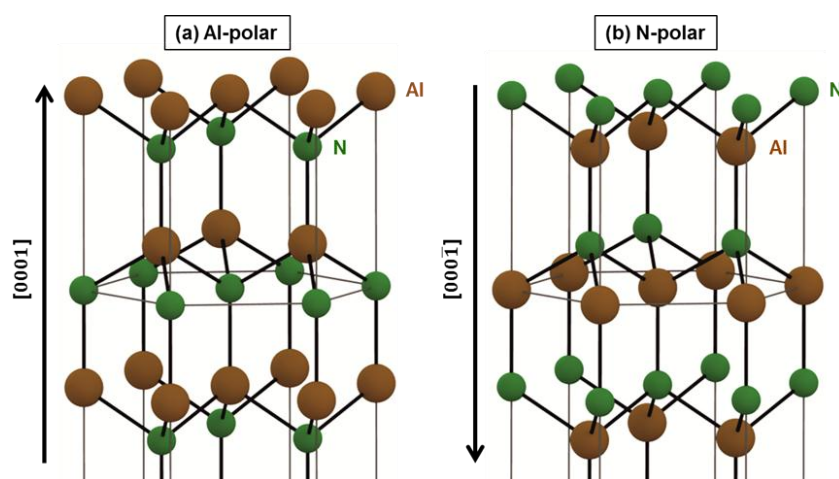


Figure 1. Models of crystal structures of (a) Al- and (b) N-polar aluminum nitride (AlN).

In this paper, we report on electrostatic self-assembly of DNPs onto differently polarized (either Al- or N-polar) *c*-axis oriented sputtered AlN film surfaces. This investigation shows that Al-polar films, as compared to N-polar ones, obtain DNPs with higher density and more homogeneously on their surfaces. The origin of these differences in density and homogeneity is discussed based on the hydrolysis behavior of AlN surfaces.

2. Results

2.1. Properties of an Aqueous Colloid of DNPs

For the electrostatic self-assembly of DNPs onto AlN film surfaces, an aqueous colloid of DNPs was prepared and its properties are mentioned below. According to analyses via dynamic light scattering (DLS), the colloidal DNPs have a narrow distribution of particle sizes centering on the core size of DNPs (~3 nm), indicating that the DNPs are monodispersed in the aqueous colloid. Also, the DNPs retain negative zeta potential of −80 mV, which is required for the successful electrostatic self-assembly of DNPs onto AlN surfaces [1]. In addition, a pH meter shows that the pH of the colloid is 6.3, where AlN surfaces most likely have positive zeta potential, which is necessary to obtain electrostatic attractive interactions between DNPs and AlN surfaces [1]. The relationship of zeta potentials between DNPs and AlN surfaces as a function of pH is discussed in Section 3 more in detail.

2.2. Densities and Distributions of DNPs Assembled onto Al- and N-Polar Sputtered AlN Film Surfaces

The electrostatic self-assembly of DNPs onto Al- and N-polar sputtered AlN film surfaces was carried out using the aforementioned aqueous colloid of DNPs. To enable clear scanning electron microscopy (SEM) observations of the DNPs assembled onto the AlN surfaces, a short-time growth of NCD grains on the AlN surfaces was additionally performed in an ellipsoidal reactor via microwave plasma assisted CVD [13]. Figure 2a,b shows the representative SEM images of the Al- and the N-polar AlN film surfaces, respectively, after the electrostatic self-assembly of DNPs plus the short-time growth of NCD grains. The white (or grey) dots and the black backgrounds in the SEM images represent NCD particles and AlN surfaces, respectively. Here, the density of NCD grains (particles) on the AlN surfaces evaluated via SEM is defined as “seed density” to make further discussions convenient. As shown in Figure 2a,b, relatively high seed densities ($\sim 10^{11} \text{ cm}^{-2}$) are homogeneously obtained on the both Al- and N-polar AlN film surfaces. However, the seed density and its homogeneity on the Al-polar film surface seem to be slightly higher than those on the N-polar film surface although those differences are not so obvious. To make this point clear, the seed densities were statistically evaluated and the results are shown in Figure 2c. The black X marks and the red circles in the figure indicate all of the measured seed densities and the averaged seed density, respectively, obtained from twenty different regions of $0.86 \mu\text{m}^2$ randomly chosen on each of the AlN film surface. As one can see in Figure 2c, there are clear differences in seed density and its homogeneity between the Al- and the N-polar film surfaces. The Al-polar film surface has higher seed density with much better homogeneity as compared to the N-polar film surface. Particularly, the minimum seed density on the Al-polar film surface ($1.08 \times 10^{11} \text{ cm}^{-2}$) is more than five times higher than that on the N-polar surface ($0.19 \times 10^{11} \text{ cm}^{-2}$). Therefore, it can now be stated that the polarity of *c*-axis oriented sputtered AlN films has an unignorable significant impact on the electrostatic self-assembly of DNPs onto AlN surfaces in terms of density and its homogeneity of the self-assembled DNPs.

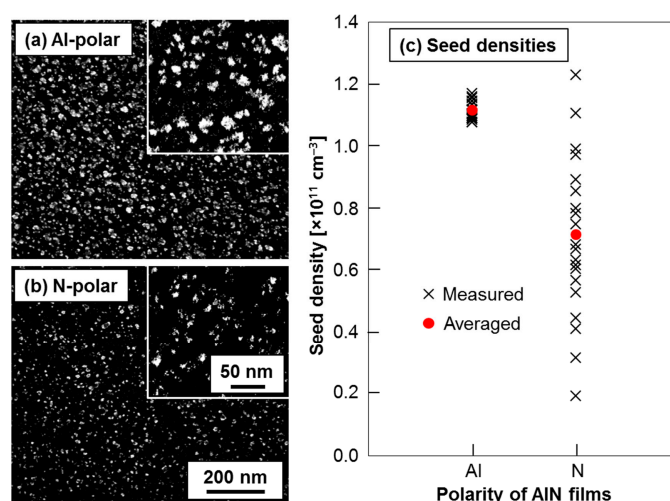


Figure 2. Representative scanning electron microscopic (SEM) images of (a) Al- and (b) N-polar AlN film surfaces after the electrostatic self-assembly of diamond nanoparticles (DNPs) plus the short-time growth of nanocrystalline diamond (NCD) grains and (c) seed densities on each polarity of AlN film surfaces determined from twenty different regions of $0.86 \mu\text{m}^2$ randomly chosen on the AlN surfaces.

2.3. Ultrathin NCD Film Growth on Al- and N-Polar Sputtered AlN Film Surfaces

In order to determine the influence of the observed differences in seed density and its homogeneity on CVD of NCD thin films, ultrathin NCD films were grown on both Al- and N-polar AlN film surfaces through the electrostatic self-assembly of DNPs. Since ultrathin NCD films are promising as transparent elastic electrode materials for emerging micro-opto-electro-mechanical system (MOEMS) applications

such as the tunable micro-optical lenses [4] introduced at the beginning, the films are expected to be very thin and pinhole-free. Now, ultrathin (~15 nm as estimated from both an in situ laser interference and a highly reproducible growth rate) NCD films were grown on both Al- and N-polar AlN film surfaces in the ellipsoidal reactor through the examined electrostatic self-assembly of DNPs onto them. The surface morphologies of the resulting ultrathin NCD films were then observed via SEM and the images are shown in Figure 3. As can be clearly seen in Figure 3, a completely coalesced homogeneous NCD film, showing very dense NCD grains and no visible pinholes, is observed on the Al-polar film surface. Meanwhile, the film grown on the N-polar film surface is not fully coalesced as many pinholes are found in the scanned area. This obvious difference in the surface morphology strongly supports the observed differences in seed density and its homogeneity between the Al- and the N-polar AlN film surfaces. Since the existence of pinholes degrades the majority of excellent properties of NCD films such as high optical transparency, high Young's modulus, high thermal conductivity, and high piezoresistivity, it can now be claimed that Al-polar films are more suitable as substrates to grow NCD thin films for all the above-introduced applications based on NCD/AlN unimorph structures.

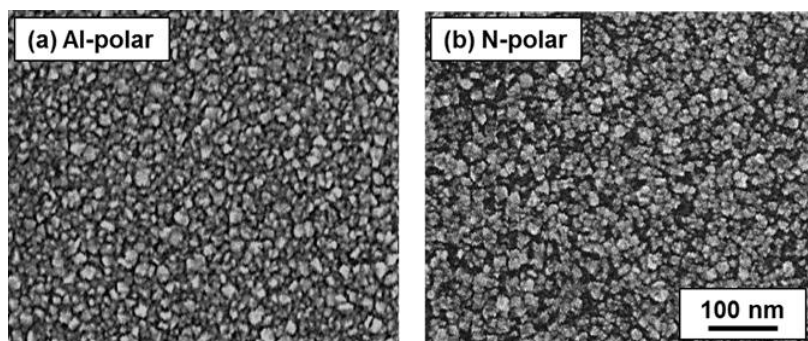
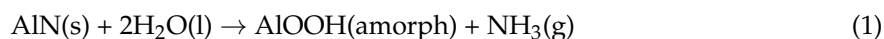


Figure 3. SEM images of ultrathin (~15 nm) NCD films grown on (a) Al- and (b) N-polar AlN film surfaces after the electrostatic self-assembly of DNPs.

3. Discussion

To track the origin of the observed differences in seed density and its homogeneity between the Al- and the N-polar AlN film surfaces, the atomic concentrations of Al, N, C and O determined via X-ray photoelectron spectroscopy (XPS) are compared between the Al- and the N-polar AlN film surfaces immediately before and after the electrostatic self-assembly of DNPs as those results are shown in Figure 4. Before the electrostatic self-assembly of DNPs, as can be seen in Figure 4a, both Al- and N-polar film surfaces show almost the same atomic concentrations of C. This probably indicates the original contaminants on the AlN film surfaces. On the other hand, the rest of atoms (Al, N and O) show different concentrations depending on the polarity of AlN films. The Al-polar film surface, as compared to the N-polar film surface, exhibits higher atomic concentrations of Al and N but much lower concentration of O for compensation. Here, the presence of oxygen atoms on AlN surfaces is mostly because of the surface oxide groups produced via the exposure of the AlN surfaces to atmospheric moisture [14], the reactions of which are described as:



Namely, the observed difference in atomic concentration of O indicates that the N-polar film surface is more oxidized in atmospheric moisture as compared to the Al-polar film surface. This is consistent with the previously reported result that N-polar AlN film surfaces oxidize more actively than

Al-polar film surfaces do [12]. Further, it is notable in Figure 4a that the ratio of atomic concentration Al/N for the N-polar film surface, that is 5.6, is more than two times higher than that for the Al-polar film surface, that is 2.1. This is understandable considering the fact that the surface oxide groups of sputtered AlN films usually originate from aluminum atoms, yielding aluminum oxide (Al_2O_3) polymorphs and hydrated aluminas, including polymorphs of aluminum oxide hydroxide (AlOOH) and aluminum trihydroxide ($\text{Al}(\text{OH})_3$) [15]. Such a different potentiality of oxidation between Al- and N-polar AlN film surfaces must be taken into account since AlN film surfaces are necessarily exposed to atmospheric moisture before performing electrostatic self-assembly of DNPs. After the electrostatic self-assembly of DNPs, as one can see in Figure 4b, the atomic concentrations of C for the both terminations of AlN surfaces are equally increased and all the rest of the atomic concentrations are reduced. This must be derived from the DNPs assembled on the AlN surfaces. The noticeable point here is that the atomic concentration of O for the N-polar film surface, which used to be much higher than that for the Al-polar film surface before the electrostatic self-assembly of DNPs, is remarkably reduced and becomes similar to that for the Al-polar film surface. As compensation for these differently reduced atomic concentrations of O, the atomic concentrations of both Al and N for the Al-polar film surface are reduced more actively in comparison to those for the N-polar film surface and finally become similar to each other.

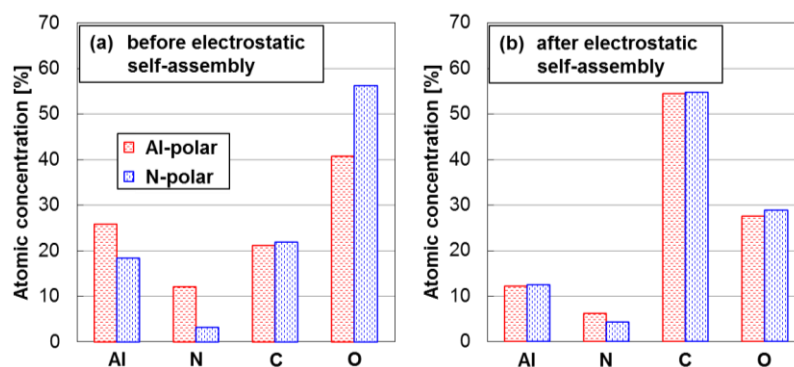


Figure 4. Atomic concentrations of Al, N, O and C on the Al- and N-polar AlN film surfaces (a) before and (b) after the electrostatic self-assembly of DNPs.

To understand this difference in reduction rate of atomic concentration of O between the Al- and the N-polar film surfaces, a general behavior of AlN surfaces in aqueous suspensions could be considered. In principle, AlN surfaces oxidize in aqueous suspensions in the same way as they do in atmospheric moisture. However, the difference is that the amorphous AlOOH layer, which is formed by reaction (1), is dissolved in aqueous suspensions and are finally precipitated as crystalline bayerite ($\text{Al}(\text{OH})_3$) [16] while such dissolved species only stay on AlN surfaces in atmospheric moisture. Therefore, the atomic concentration of O on the N-polar film surface, accumulated in atmospheric moisture more than that on the Al-polar film surface, would more actively be reduced via the electrostatic self-assembly of DNPs by dissolving higher amount of AlOOH groups in the aqueous colloid of DNPs. The point here is that such a stronger hydrolysis behavior of the N-polar film surface, in comparison to the Al-polar film surface, more drastically increases the pH of the aqueous colloid as AlN hydrolyzes by accepting protons or releasing hydroxyl ions [17]. Consequently, the zeta potentials of both DNPs and AlN surfaces in the aqueous colloid would be changed. Here, the zeta potentials of the air-annealed DNPs and as-received AlN nanopowder are plotted in Figure 5 as a function of pH of the aqueous suspensions. The dashed line in Figure 5 indicates the pH (~6.3) of the aqueous colloid used for the electrostatic self-assembly of DNPs. As can be seen in Figure 5, the air-annealed DNPs show relatively high negative zeta potential of < -60 mV over a wide range of pH, and this tendency is consistent with previous studies [1,18,19]. Meanwhile, the AlN nanopowder shows the positive zeta potential of ~ 50 mV at the pH of below ~ 6 but the zeta potential drastically

decreases with increasing pH; this tendency has an agreement with previously reported results [1,17]. Considering such a drastic downward trend of the zeta potential of AlN with increasing pH, the N-polar film surface, which retains higher amounts of Al–OH groups than the Al-polar film surface does in atmospheric moisture, would cause lower positive zeta potentials in the aqueous colloid by following the aforementioned hydrolysis mechanism. Since such a drop in positive zeta potentials of AlN film surfaces necessarily results in weaker electrostatic attractive interactions with DNPs retaining negative zeta potentials, it can now be concluded that Al-polar AlN film surfaces, as compared to N-polar film ones, obtain higher seed density more homogeneously due to their less active oxidation in atmospheric moisture and also more refrained hydrolysis behavior in aqueous colloids of DNPs. Although any in situ analysis of AlN film surfaces and pH of an aqueous colloid during the electrostatic self-assembly of DNPs could not have been performed in this study due to its technical difficulties, the performed experiments and the previously reported statements well explain the observed differences in seed density and its homogeneity between Al- and N-polar AlN film surfaces.

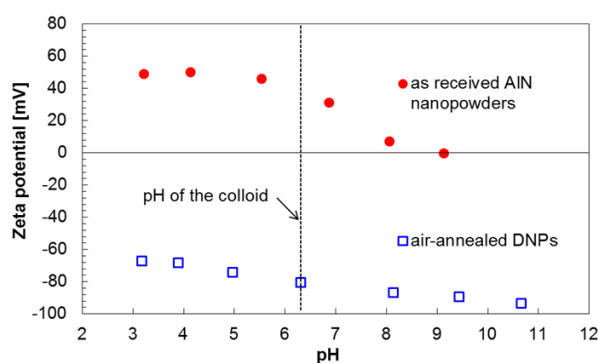


Figure 5. Zeta potentials of air-annealed DNPs and as-received AlN nanopowders in deionized (DI) water as a function of pH.

4. Materials and Methods

4.1. Materials

In this study, commercially available detonation nanodiamond powder (Plasmachem GmbH, Berlin, Germany, grade G01) and AlN nanopowder (593044-10G, Sigma Aldrich, St. Louis, MO, USA) were used to produce their aqueous colloids. The surfaces of AlN films used in this study, for both Al- and N-polar cases, were the surfaces of highly *c*-axis oriented AlN films sputtered on Si(100) substrates. The sputtered Al- and N-polar AlN films show, as an evidence of the polarity difference, opposite signs in longitudinal piezoelectric coefficients (d_{33}) of $\sim +6$ and ~ -4 pm/V, respectively. Also, the Al- and the N-polar films show huge differences in both etching rates in an aqueous KOH solution and etched surface morphologies [20]. Here, it should be mentioned that each polarity of the AlN films were sputtered with the same sputtering process parameters described elsewhere [21] but in different radio frequency (RF) magnetron sputtering systems providing different background (base) pressures. Although the origin of the obtained polarity difference is not very obvious due to its complexity, the difference of background pressure can be one of the origins; it has been reported that even a very small difference in oxygen concentration in sputtering atmosphere inverts the polar direction of the resulting AlN films [22].

4.2. Methods

The detonation nanodiamond powder was initially annealed in air in order to obtain a negative zeta potential in an aqueous colloid, which is required for the successful electrostatic self-assembly of DNPs onto AlN surfaces [1]. The annealing temperature was maintained at 450 °C for 8 h in atmospheric pressure. An aqueous suspension containing air-annealed DNPs was then made by

immersing 1.0 g of the annealed powder into 200 mL of deionized (DI) water. To make the DNPs well-dispersed in the suspension and make their sizes minimized, the suspension was ultrasonicated with a high-power ultrasonic horn for 4 h and centrifuged with relative centrifugal force of over 40 kg for 8 h, respectively. The resulting aqueous colloid of DNPs was characterized in terms of particle size and zeta potential using a DLS apparatus (Malvern Instruments, Malvern, Worcestershire, UK, Zetasizer Nano ZS) equipped with a 633 nm laser. The particle size and the zeta potential, respectively, were determined from the average of 100×30 s scans in the back-scattering configuration (173°). Further, the pH of the colloid was checked using a pH meter (SG2, Mettler Toledo, Columbus, OH, USA). The aqueous colloid of AlN nanopowder was also prepared via the same procedure for the DNPs (without annealing in air) and characterized in terms of zeta potential and pH. To perform the electrostatic self-assembly of DNPs onto the differently polarized AlN film surfaces, the surfaces of both Al- and N-polar AlN films were firstly immersed into the colloid of DNPs in an ultrasonic bath for 5 min. The AlN surfaces were subsequently rinsed in DI water to leave only electrostatically self-assembled DNPs on the AlN surfaces and then were dried under a gentle flow of nitrogen gas. To enable clear SEM observations of the DNPs assembled onto the AlN surfaces, a short-time growth of NCD grains on the AlN surfaces was additionally performed in an ellipsoidal reactor via microwave plasma assisted CVD [13]. The short-time growth conditions were 2500 W microwave power, 640°C substrate temperature, 30 Torr process pressure, 4% methane diluted by hydrogen, and 10 min growth duration. After the short-time growth, the AlN surfaces were assessed via SEM (REM4500, Hitachi, Tokyo, Japan) in order to evaluate densities and distributions of the DNPs remaining on them. In order to discuss about the influence of the polarity of AlN films on the resulting densities and distributions of DNPs, XPS (homemade apparatus) was performed on the differently polarized AlN film surfaces immediately before and after the electrostatic self-assembly of DNPs. The XPS was performed using a monochromatized Al $K\alpha$ anode (1486.6 eV) calibrated versus the Au $4f_{7/2}$ peak located at 84.0 eV. The spectrometer was equipped with a hemispherical energy analyzer (EA 125, Scienta Omicron, Taunusstein, Hessen, Germany). The path energy was 20 eV corresponding to an energy resolution of 0.6 eV. This XPS set-up was previously used to investigate DNPs assembled onto various substrates [23–25]. Although the serious charging of the AlN surfaces and DNPs unfortunately disabled reasonable characterizations of chemical bonds on the AlN surfaces, the atomic concentrations of Al, N, C and O on the differently polarized AlN film surfaces are accurately compared before and after the electrostatic self-assembly of DNPs. The atomic concentrations were calculated from XPS spectra after corrections by the photo-ionization cross-sections. Areas of the corresponding XPS core levels were obtained after a Shirley correction of the background.

5. Conclusions

In this study, electrostatic self-assembly of DNPs was examined onto differently polarized (either Al- or N-polar) *c*-axis oriented sputtered AlN film surfaces. Also, ultrathin (~ 15 nm) NCD films were grown on both polarities of AlN film surfaces via the examined electrostatic self-assembly of DNPs. Further, the behaviors of differently polarized AlN film surfaces in atmospheric moisture and aqueous suspensions were discussed based on the atomic concentrations of Al, N, C and O on the surfaces determined via XPS before and after the electrostatic self-assembly of DNPs. These investigations and discussions provided one conclusion that Al-polar AlN film surfaces, as compared to N-polar film ones, obtain higher seed density more homogeneously due to their less active oxidation in atmospheric moisture and also more refrained hydrolysis behavior in aqueous colloids of DNPs. Therefore, it can be claimed that Al-polar films are more suitable as substrates to grow NCD thin films for the applications based on NCD/AlN unimorph structures such as surface acoustic wave resonators, mechanical micro-resonators, and tunable micro-optical lenses.

Acknowledgments: The authors would like to thank Georgia Lewes-Malandrakis and Michaela Fritz for the technical assistance and to acknowledge funding from the German Research Foundation (DFG).

Author Contributions: Taro Yoshikawa and Verena Zuerbig conceived and designed the experiments; Taro Yoshikawa, Markus Reusch, Kee-Han Lee, Magdalena Kurzyp and Jean-Charles Arnault performed the experiments; Taro Yoshikawa and Jean-Charles Arnault analyzed the data; Volker Cimalla, Jean-Charles Arnault, Christoph E. Nebel, Oliver Ambacher and Vadim Lebedev contributed reagents/materials/analysis tools; Taro Yoshikawa wrote the paper.

Conflicts of Interest: The authors declare no conflict of interest.

Abbreviations

The following abbreviations are used in this manuscript:

CVD	Chemical vapor deposition
NCD	Nanocrystalline diamond
AlN	Aluminum nitride
DLS	Dynamic light scattering
SEM	Scanning electron microscope
MOEMS	Micro-opto-electro-mechanical system
XPS	X-ray photoelectron spectroscopy
DI	Deionized

References

1. Hees, J.; Heidrich, N.; Pletschen, W.; Sah, R.E.; Wolfer, M.; Williams, O.A.; Lebedev, V.; Nebel, C.E.; Ambacher, O. Piezoelectric actuated micro-resonators based on the growth of diamond on aluminum nitride thin films. *Nanotechnology* **2013**, *24*, 025601. [[CrossRef](#)] [[PubMed](#)]
2. Bénédic, F.; Assouar, M.B.; Mohasseb, F.; Elmazria, O.; Alnot, P.; Gicquel, A. Surface acoustic wave devices based on nanocrystalline diamond and aluminium nitride. *Diam. Relat. Mater.* **2004**, *13*, 347–353. [[CrossRef](#)]
3. Heidrich, N.; Iankov, D.; Hees, J.; Pletschen, W.; Sah, R.E.; Kirste, L.; Zuerbig, V.; Nebel, C.; Ambacher, O.; Lebedev, V. Enhanced mechanical performance of AlN/nanodiamond micro-resonators. *J. Micromech. Microeng.* **2013**, *23*, 125017–125022. [[CrossRef](#)]
4. Zuerbig, V.; Pletschen, W.; Hees, J.; Sah, R.E.; Kirste, L.; Heidrich, N.; Nebel, C.E.; Ambacher, O.; Lebedev, V. Transparent diamond electrodes for tunable micro-optical devices. *Diam. Relat. Mater.* **2013**, *38*, 101–103. [[CrossRef](#)]
5. Godbole, V.P.; Jagannadham, K.; Narayan, J. Nucleation and growth of diamond films on aluminum nitride coated nickel. *Appl. Phys. Lett.* **1995**, *67*, 1322–1324. [[CrossRef](#)]
6. Cui, J.B.; Ma, Y.R.; Zhang, J.F.; Chen, H.; Fang, R.C. Growth and characterization of diamond film on aluminum nitride. *Mater. Res. Bull.* **1996**, *31*, 781–785. [[CrossRef](#)]
7. Wang, W.L.; Zhang, R.Q.; Liao, K.J.; Sun, Y.W.; Wang, B.B. Nucleation and growth of diamond films on aluminum nitride by hot filament chemical vapor deposition. *Diam. Relat. Mater.* **2000**, *9*, 1660–1663. [[CrossRef](#)]
8. Pobedinskas, P.; Degutis, G.; Dexters, W.; Janssen, W.; Janssens, S.D.; Conings, B.; Ruttens, B.; D’Haen, J.; Boyen, H.G.; Hardy, A.; et al. Surface plasma pretreatment for enhanced diamond nucleation on AlN. *Appl. Phys. Lett.* **2013**, *102*, 201609–201612. [[CrossRef](#)]
9. Reddy, P.; Bryan, I.; Bryan, Z.; Guo, W.; Hussey, L.; Collazo, R.; Sitar, Z. The effect of polarity and surface states on the Fermi level at III-nitride surfaces. *J. Appl. Phys.* **2014**, *116*, 123701–123706. [[CrossRef](#)]
10. Zhuang, D.; Edgar, J.H.; Strojek, B.; Chaudhuri, J.; Rek, Z. Defect-selective etching of bulk AlN single crystals in molten KOH/NaOH eutectic alloy. *J. Cryst. Growth* **2004**, *262*, 89–94. [[CrossRef](#)]
11. Zhuang, D.; Edgar, J.H. Wet etching of GaN, AlN, and SiC: A review. *Mater. Sci. Eng. R Rep.* **2005**, *48*, 1–46. [[CrossRef](#)]
12. Gu, Z.; Edgar, J.H.; Speakman, S.A.; Blom, D.; Perrin, J.; Chaudhuri, J. Thermal oxidation of polycrystalline and single crystalline aluminum nitride wafers. *J. Electron. Mater.* **2005**, *34*, 1271–1279. [[CrossRef](#)]
13. Yoshikawa, T.; Gao, F.; Zuerbig, V.; Giese, C.; Nebel, C.E.; Ambacher, O.; Lebedev, V. Pinhole-free ultra-thin nanocrystalline diamond film growth via electrostatic self-assembly seeding with increased salt concentration of nanodiamond colloids. *Diam. Relat. Mater.* **2016**, *63*, 103–107. [[CrossRef](#)]

14. Bowen, P.; Highfield, J.G.; Mocellin, A.; Ring, T.A. Degradation of aluminum nitride powder in an aqueous environment. *J. Am. Ceram. Soc.* **1990**, *73*, 724–728. [[CrossRef](#)]
15. Dalmau, R.; Collazo, R.; Mita, S.; Sitar, Z. X-ray photoelectron spectroscopy characterization of aluminum nitride surface oxides: Thermal and hydrothermal evolution. *J. Electron. Mater.* **2007**, *36*, 414–419. [[CrossRef](#)]
16. Mobley, W.M. Colloidal Properties, Processing and Characterization of Aluminum Nitride Suspensions. Ph.D. Thesis, Alfred University, Alfred, NY, USA, 1996.
17. Krnel, K.; Kosmač, T. Reactivity of aluminum nitride powder in dilute inorganic acids. *J. Am. Ceram. Soc.* **2000**, *83*, 1375–1378. [[CrossRef](#)]
18. Williams, O.A.; Hees, J.; Dieker, C.; Jäger, W.; Kirste, L.; Nebel, C.E. Size-dependent reactivity of diamond nanoparticles. *ACS Nano* **2010**, *4*, 4824–4830. [[CrossRef](#)] [[PubMed](#)]
19. Hees, J.; Kriele, A.; Williams, O.A. Electrostatic self-assembly of diamond nanoparticles. *Chem. Phys. Lett.* **2011**, *509*, 12–15. [[CrossRef](#)]
20. Zhuang, D.; Edgar, J.H.; Liu, L.; Liu, B.; Walker, L. Wet chemical etching of AlN single crystals. *MRS Int. J. Nitride Semicond. Res.* **2002**, *7*, 4–6.
21. Reusch, M.; Holc, K.; Pletschen, W.; Kirste, L.; Žukauskaite, A.; Yoshikawa, T.; Iankov, D.; Ambacher, O.; Lebedev, V. Analysis and optimization of sputter deposited AlN-layers for flexural plate wave devices. *J. Vac. Sci. Technol. B* **2016**, *34*, 052001. [[CrossRef](#)]
22. Akiyama, M.; Kamohara, T.; Kano, K.; Teshigahara, A.; Kawahara, N. Influence of oxygen concentration in sputtering gas on piezoelectric response of aluminum nitride thin films. *Appl. Phys. Lett.* **2008**, *93*, 021903. [[CrossRef](#)]
23. Arnault, J.C.; Saada, S.; Williams, O.A.; Haenen, K.; Bergonzo, P.; Nesladek, M.; Polini, R.; Osawa, E. Diamond nanoseeding on silicon: Stability under H₂ MPCVD exposures and early stages of growth. *Diam. Relat. Mater.* **2008**, *17*, 1143–1149. [[CrossRef](#)]
24. Zeppilli, S.; Arnault, J.C.; Gesset, C.; Bergonzo, P.; Polini, R. Thermal stability and surface modifications of detonation diamond nanoparticles studied with X-ray photoelectron spectroscopy. *Diam. Relat. Mater.* **2010**, *19*, 846–853. [[CrossRef](#)]
25. Petit, T.; Girard, H.A.; Trouvé, A.; Battonneau-Gener, I.; Bergonzo, P.; Arnault, J.C. Surface transfer doping can mediate both colloidal stability and self-assembly of nanodiamonds. *Nanoscale* **2013**, *5*, 8958–8962. [[CrossRef](#)] [[PubMed](#)]



© 2016 by the authors; licensee MDPI, Basel, Switzerland. This article is an open access article distributed under the terms and conditions of the Creative Commons Attribution (CC-BY) license (<http://creativecommons.org/licenses/by/4.0/>).